New system design for the cultivation of extractive species at exposed sites - Part 2: Experimental modelling in waves and currents

Jannis Landmann [a,*], Lukas Fröhling [a], Rebekka Gieschen [b], Bela H. Buck [c,d], Kevin Heasman [e], Nicholas Scott [e], Malcolm Smeaton [e], Nils Goseberg [b,f], Arndt Hildebrandt [a]

[a] Leibniz Universität Hannover, Ludwig-Franzius-Institute for Hydraulic, Estuarine and Coastal Engineering, Nienburger Straße 5, 30167 Hannover, Germany
[b] Leichtweiß-Institut for Hydraulic Engineering and Water Resources, Division Hydromechanics, Coastal and Ocean Engineering, Technische Universität Braunschweig, Beethovenstr. 51a, 38106 Braunschweig, Germany
[c] Alfred Wegener Institut, Helmholtz-Zentrum für Polar- und Meeresforschung, Bussestr. 27, 27570 Bremerhaven, Germany
[d] Applied Marine Biology and Aquaculture, University of Applied Sciences Bremerhaven, An der Karlstadt 8, 27568 Bremerhaven, Germany
[e] Cawthron Institute, 98 Halifax Street East, Nelson 7010, New Zealand
[f] Coastal Research Center, Joint Research Facility of Leibniz Universität Hannover and Technische Universität Braunschweig, Hannover, Germany

ARTICLE INFO

ABSTRACT

Aquaculture is projected to be a major supplier of marine proteins to large parts of the global population. This includes bivalves, which have a high potential to offset protein deficits, as they are highly adaptable to varying water temperature, salinity, desiccation, and oxygen conditions. This work is part of a two-piece contribution on novel marine aquaculture technology and details physical laboratory tests of a new cultivation system for bivalve farming called "*Shellfish Tower*". The tested 1:20 model consists of a rectangular cage (2×2 m prototype scale) with a central buoyancy element and a height of $2 - 4$ m. Testing was done in a current flume as well as a wave basin for current velocities between $0.4 - 2.2$ m/s and wave heights of 1.6 to 5.0 m with periods between 5 to 14 s. The tests were conducted to prove the feasibility and functionality of this aquaculture system, which is usable for the collection and cultivation of mussel spat as well as for the grow-out of oysters, scallops, and seaweed in marine environments. Tests carried out in a current flume revealed that drag coefficients decrease with increasing current velocities, and range from $C_d=0.5$ to 2.5, while the mooring inclination increases from 12° to 84° with increasing flow velocity, which is highly dependant on the buoyancy related pretension. The examination of the mooring line tensions recorded in a wave basin showed that the largest values of snap-induced tension were up to 10 times that of the semi-static tension. The maximum-recorded tension on the system was 48 kN for a single and 89 kN for a double configuration, compared to non-snap tension values, which were in the range of $6 - 10$ kN. The insights gathered in this study will inform the future design of aquaculture systems in high-energy environments and allow for an integration into numerical models.

1. Introduction

To date, shellfish farming in New Zealand and across the world predominantly takes place in sheltered inshore or nearshore farms. In New Zealand, a well-established shellfish industry produces up to 100,000 t of greenshell™ mussels (*Perna canaliculus*) and 2000 t of Pacific Oysters (*Magallana gigas*) per annum (FAO 2020), all of which is produced in sheltered waters. Inshore systems produce mussels on a continuous mussel production rope referred to as a *longline* (Dawber, 2004, Hickman, 1992, Buck, 2007, Cheney et al., 2010) (cp. Fig. 1). Oysters are produced in baskets on racks or similar structures in shallow

tidal waters. The aquaculture industry is however expanding into exposed waters off the coast in the Bay of Plenty and Hawke's Bay (North Island) as well as at Pegasus Bay, D'Urville Island and in the Cook Strait (South Island) (New Zealand Government 2017). The New Zealand Government supports this expansion and believes there is potential for a five-fold increase in annual aquaculture sales by 2035 (New Zealand Government 2019). There is abundant space in the exposed ocean within the exclusive economic zone around New Zealand as discussed in Heasman et al. (2020). These exposed sites have demanding physical, oceanographic, and biological conditions and existing farming technology developed for protected areas cannot simply be copied and extended here. Innovative, robust systems and mooring designs that can

Notation

Symbol Appellation Dimension

ECDF	Empirical cumulative distribution function	[-]
h_{char}	Characteristic model height	[m]
C_D	Drag coefficient	[-]
D	Model diameter	[m]
F_A	Buoyancy Force	[N]
F_G	Mass Force	[N]
$F_{Magnitude}$	Magnitude Force	[N]
F_{Pre}	Pretension Force	[N]
F_x	Force in x-direction	[N]
F_y	Force in y-direction	[N]
F_z	Force in z-direction	[N]
Hs	Significant wave height	[m]
a_{mag}	Acceleration	[m/s^2]
u	Current velocity	[m/s]
α	Current-induced angle	[°]
β	Model orientation angle	[°]
γ	Inclination angle of mooring	[°]
$F_{Horizontal}$	Horizontal force	[N]

be submerged during high-energy storm events must be developed to evade high-energetic forces closer to the surface. For this reason, New Zealand Ministry of Business, Innovation and Employment (MBIE) has financed a project led by the Cawthron Institute, to develop new technologies that meet these conditions (Heasman et al., 2020). The primary aim of this project was to develop an easy-to-use aquaculture system (during deployment, operations, and harvesting) that could withstand 0.8 m/s currents and waves of 7 m significant wave height and 11 to 14 s period. The, so called, "*Shellfish Tower*" was designed to address this aim. It is a submersible cage system suitable for the collection and cultivation of mussel spat as well as grow out of oysters, scallops, and seaweed. The system and its iterative design process are presented in the companion paper by Heasman et al. (2021) (this issue). There a system analysis for the Shellfish Tower as a new cultivation technology for exposed bivalve farming is performed and the technical feasibility is assessed. The development is highlighted from the system design over the fabrication to the deployment at sea. The physical model tests described in this study supported the design process. The final prototype structure has a hexagonal form with a cylindrical buoyancy element with a diameter of 1.08 m in the centre. The hexagonal frame of the system is 2.4 m high, including the bracing at the top and the mooring mechanism at the bottom and has a diameter of 2.7 m. In the corners of the hexagon, six sub-units for the cultivation of oysters as well as for the collection of mussel spat are located. Each sub-unit consists of a 1.91 m high rectangular cage with a diameter of 1.0 m. The whole structure has a diameter of 4.6 m at the widest point from the corner of the subunits to the other and weighs 1100 kg in air. The prototype system is single moored to a screw anchor in a depth of 45 m, six nautical miles off the Bay of Plenty, North Island (New Zealand), in exposed waters near a commercial mussel farm and has been in test mode since then. The

results of Heasman et al. (2021) indicate a design tolerance for significant wave heights of over 7 m and currents of over 0.8 m/s.

Scientists have been developing concepts for the cultivation of plants and animals in offshore environments since the late 1970s (Hanson, 1974, Bugrov et al., 1994, Buck, 2004) yet few operational systems currently exist (cp. Fig. 1). This is true not only for the production of aquatic food but also regarding the cultivation of plants as an energy resource (Cannon, 1980). Moreover, few works exist that detail the design process of open ocean aquaculture systems or offer guidance on how to optimise this process. It is therefore important to prepare literature on the development of novel systems for offshore aquaculture integrated with and underpinned by modern engineering principals to facilitate future innovation and growth of the industry. All that said, in recent years there have been works from which one could draw knowledge. Goseberg et al. (2017) discuss the requirements of offshore aquaculture technology using case studies but do not discuss how they should be addressed. Their work advocated for multi-use systems which is supported by Dalton et al. (2019) who present a review and summary of the financial and technological benefits from ocean-based multi-use systems. Lagasco et al. (2019) present a study detailing a wave-powered fin-fish farm based on the design goals of optimising fish production, minimising pollution, and maximising energy generation in open ocean conditions. Using a combination of numerical modelling, field testing and analytical modelling, Buck and Langan (2017) detail the development process of an offshore mussel longline connection suitable to attach to existing monopiles and a sample tripod.

Beyond these works one must draw from literature specific to individual aspects of open ocean aquaculture such as offshore potential analysis (Cheney et al., 2010), system engineering (Kim et al., 2014, Lader et al., 2007, C.-W. C.-W. Bi et al., 2020), aquaculture site-selection (Benetti et al., 2010), hydrodynamic parameters of aquaculture species (Hildebrandt et al., 2018, Plew et al., 2009, Gagnon, 2019, Landmann et al., 2019, Gansel et al., 2015) and monitoring telemetry devices for operations and maintenance (Irish et al., 2004). Potentially hazardous force peaks on mooring systems introduced by snap loads have to be considered as well. The phenomenon of snap loads has been investigated in physical (Bardestani and Faltinsen, 2013) as well as numerical model tests (Hsu et al., 2018, Palm et al., 2013, Palm et al., 2017, Palm and Eskilsson, 2020). Hsu et al. (2017) conducted physical model tests on a semi-submersible floating offshore wind platform under currents, waves and wind. These authors suggest that an inclusion of snap-induced tension maxima in ultimate limit state evaluations could be beneficial. Qiao et al. (2020) investigated the occurrence and conditions for snap loads in mooring lines through the calculation of dynamic tension under different excitation parameters and influence factors. They concluded that higher pre-tension provides a benefit for avoiding snap loads in mooring lines. Despite these hints from literature, it is still difficult to provide a clear, complete pathway and set of recommendations to practitioners, technology developers and academics that facilitates the design process from an idea to a deployed system prototype. This is because every site is subject to its own unique conditions and every aquaculture organism has its own site selection criteria and system design requirements. Longline system designs are considered as the most promising in regard to an expansion to open ocean or exposed areas (Cheney et al., 2010, Buck and Langan, 2017) and a number of valuable
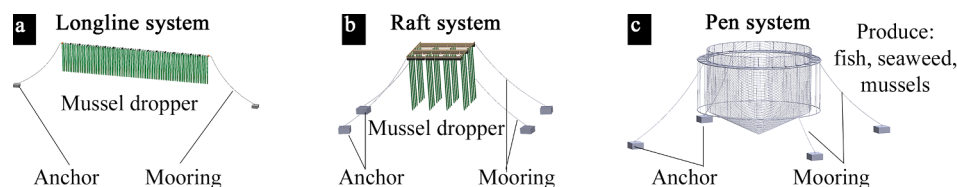

Fig. 1. Overview of marine aquaculture systems with longline- (a) and raft-systems (b) used for the industrial-scale cultivation of mussels as well as a schematic sketch of a marine pen-system usable for multi-species cultivation (c).

studies based on field experiments as well as numerical studies are available. Raman-Nair and Colbourne (2003) and Raman-Nair et al. (2008) created a numerical model for the prediction of motion as well as forces for submerged longline systems based on Kane and Levinson (1985) and the Morison et al. (1950). Supported by hydrodynamic coefficients, which need to be pre-determined, it can be used for the optimization and modification of existing and planned longline aquaculture designs under steady flow conditions. Zhao et al. (2019) tested lantern nets suspended from longlines to investigate their hydrodynamic response and analyse the influence of the system layout on the tension within the mooring line, the movement of the mainline and the lantern net itself. A more recent numerical study by Cheng et al. (2020) incorporates oscillatory flows, i.e. tides, circulation and waves, in a dynamic model to simulate the motion of the longline based on the lumped mass method. Forces on the model components are again determined according to Morison et al. (1950). The lumped mass method was also used by Huang et al. (2006) and Huang and Pan (2010) to investigate anchoring fatigue and perform a risk analysis of a single-point anchored cage culture system. In a study by Knysh et al. (2020), the fluid-structure interactions of a longline system are analysed via finite element methods and an equivalent mussel dropper was introduced for incorporation into numerical models. Numerical experiments regarding the interaction between flow and flexible nets used in aquaculture by Bi et al. (2014) and physical experiments regarding the drag on and flow through nets under currents (Bi et al., 2018) as well as waves (Bi et al., 2020) yielded drag and inertia coefficients. Field observations regarding the impact of longline farms on current reduction, stratification and wave attenuation have been conducted by Plew et al. (2005). The hydrodynamic loads on an existing longline system have been observed by Stevens et al. (2007). They noted that, while oscillatory tidal motions are the main contributor to the mean force, waves and currents can increase the maximum load by more than 100%. The forces and motion of a submerged longline system at an offshore site were observed by Gagnon and Bergeron (2017) and a growth model to estimate the average envelope diameter and linear buoyant weight of dropper lines was proposed.

In the light of the various segmented findings in literature so far, this work will attempt to use comprehensive experimental modelling to foster the procedural design chain. The general objective of the present study is to:

- prove the feasibility and functionality of an aquaculture system usable for the collection and cultivation of mussel spat as well as grow out of oysters, scallops and seaweed in marine environments using comprehensive tests conducted under laboratory conditions.

The specific objectives, which are conducted in the context of this work, are:

- an assessment and a presentation of the data processing methods used and the selection of measurement sections adhering to the state of science.
- an evaluation of the results regarding the influence of currents and waves on varying model setups with a focus on environmental loads and system movement.
- a discussion on the influence of snap loads and the implications for further research while providing general observations for cage-based marine bivalve structures and farm setups in offshore locations.

To this end, physical experiments are conducted in a 1:20 scale to identify potential weak spots and help the development of the overall system. The paper in conjunction with the work of Heasman et al. (2020) (this issue) highlights the applied benefits of using physical experiments to develop a practical outcome.

2. Material & methods

Physical model tests were conducted in two facilities of the collaborating institutions. The inclined current flume of the Leichtweiß-Institut for Hydraulic Engineering and Water Resources, Division Hydromechanics, Coastal and Ocean Engineering, Technische Universität Braunschweig was used to determine the influence of the current on the structure (cp. Fig. 2a). The flume is 36.4 m long, 2.0 m wide and 0.8 m high. The maximum flow velocity depends on the settings of the inflow control weir, connected pumps and inclination of the flume. The second set of tests, looking at the influence of waves and currents were conducted in the 3D-wave and current basin of the Ludwig-Franzius-Institute for Hydraulic, Estuarine and Coastal Engineering, Leibniz Universität Hannover (cp. Fig. 2b). The basin is 40 m long, 24 m wide and has a maximum water depth of 1.0 m. The generation of regular as well as irregular waves via a 3D snake wave maker with 72 individual wave paddles is possible. Maximal attainable wave heights are 0.47 m with possible wave spreading from 5° to 175° Three pumps with a capacity of 5.0 m³/s generate a maximum current velocity of 0.5 m/s with a water level set to 1.0 m. Fig. 2 shows a schematic view of both facilities with an indication of current and wave generation as well as model placement.

2.1. Physical model

The tested system represents an iterative step in the design process of the *Shellfish Tower* and varies from the final prototype design described in the introduction. The model consisted of a 2.0 m rectangular cage (prototype scale) with a central buoyancy element and four spaces for sub-units in the corners. The subunits are used for the cultivation of crop. The physical model tests were conducted in a 1:20-scale and Froude similarity was applied. The model was tested as a single cage with a 0.1 m model height as well as a cage of doubled height corresponding to 0.2 m model height. The 0.04 m wide subunits were connected to the frames with 1 mm steel rods. The buoyancy element was modelled by a cylindrical buoyancy tank with a radius of 0.04 m. The lateral area of the subunits was filled to account for the increase in area and drag when crop is growing on the system. Custom-made Styrofoam bodies with a density of 0.06 g/cm³ were used to compensate for the resulting additional weight to achieve the desired buoyancy. To avoid additional buoyancy through enclosed air, holes were added to the subunits for excess air to escape. The model was produced via selective laser sintering out of glass-fibre reinforced polyamides with a density of 1.22 g/cm³. The mooring line, as the connection between model structure and force transducer, consists of a 2 mm Dyneema© SK78 fibre, with a working elongation of <1% and high durability with a breaking load of 410 kg. The mooring line was attached to the bottom of the model via a noose knot around the centre of the bottom frame, with the remainder of the fibre hanging loose. To the loose end, the actual mooring line was attached via a Carrick Bend, a secure rope joint. The length of the mooring line was chosen so that the model was completely submerged, with a distance of 0.01 m between the model and the still water level. Based on the mass and volume of the two structures, the mass force and buoyancy force could be calculated, as well as the pretension resulting from the difference between them. Table 1 gives an overview regarding the static forces acting on the single and double model. Fig. 3 shows the complete structures with cuboid subunits as single cage, as a double cage as well as in a design sketch.

2.2. Current tests

To measure the forces exerted on the system through current activity as well as the deflection of the cage system with a single mooring, experiments were conducted in the inclined current flume. The experiments were carried out with a constant water depth of 0.4 m for the single cage size and 0.5 m for the double cage size, respectively, which
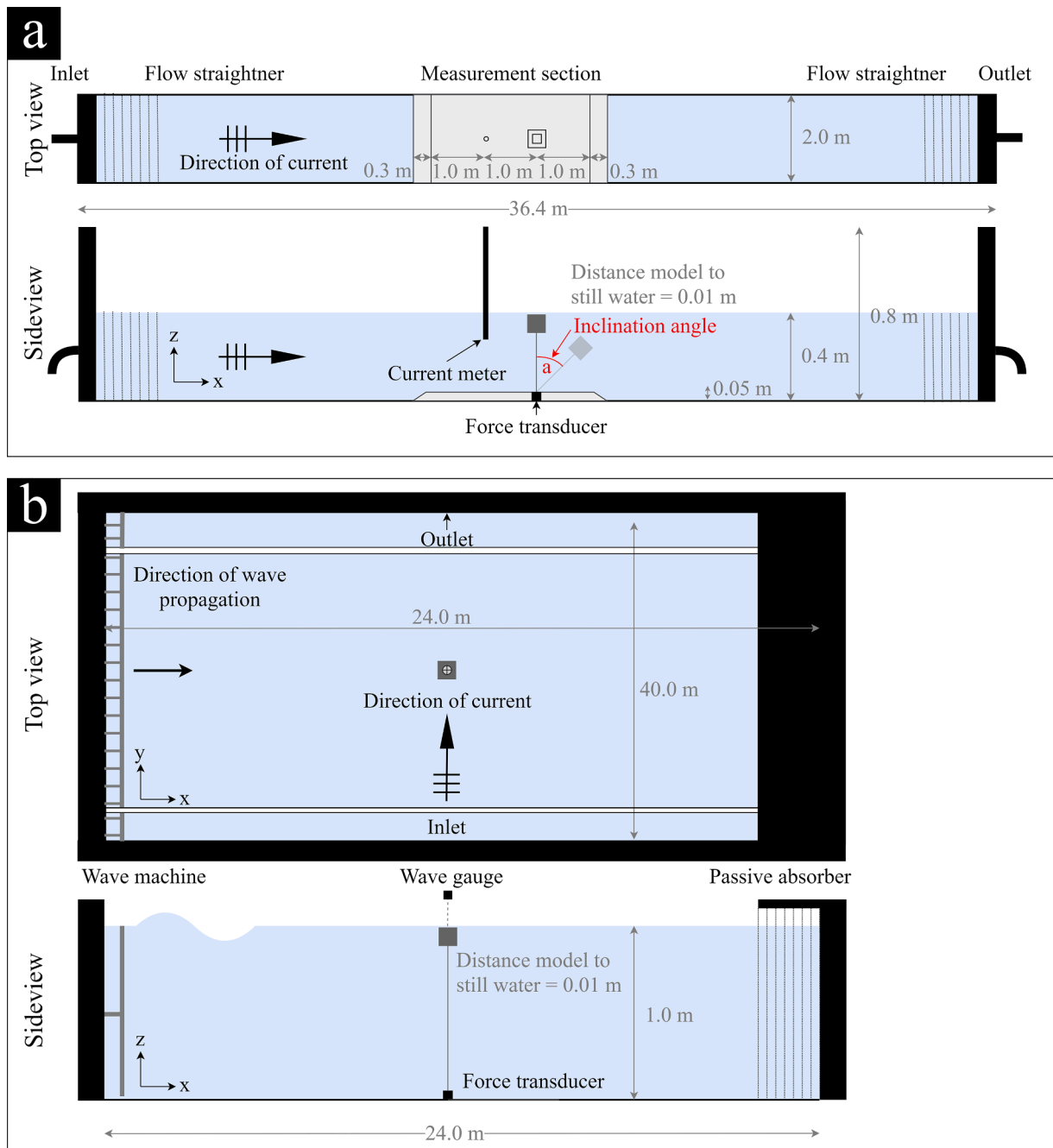
Fig. 2. Schematic top and side view of the inclined current flume of the division of Hydraulic Engineering and River Morphology of the Leichtweiß-Institute, Technische Universität Braunschweig with an indication of the used measurement equipment (a) as well as a top and side view of the 3D-wave and current basin of the Ludwig-Franzius-Institut, Leibniz Universität Hannover with an indication of the used measurement equipment (b). Not to scale.

Table 1
Overview of different model setups in regard to cage height (single & double) with an indication of volume, mass, mass force, buoyant force and pretension in the mooring.

Cage size	Single (Model height: 0.1 m)	Double (Model height: 0.2 m)
Volume [cm^3]	460.33	920.66
Mass [g]	376.25	752.50
Mass Force F_G [N]	3.69	7.38
Buoyancy Force F_A [N]	4.50	9.00
Pretension F_{Pre} [N]	0.81	1.62

corresponds to 20 m and 25 m in prototype scale. At the location of the prototype a water depth of 45 m was measured, which was not possible to recreate in the flume, as the desired current velocities could not be attained with a higher water level. The model was moored to a three-axis-force-transducer (K3D120, ME-Meßsysteme GmbH, Henningsdorf, Germany) attached to the bottom of the flume. The force transducer has a nominal force range of up to 200 N in x-, y- and z-direction and a sensitivity of 0.4 N. The x-direction corresponds to a movement from the point of origin in the current direction; the y-direction represents a movement from the point of origin to the right flume panel while the z-direction is described by a movement from the point of origin towards the top of the basin. The sample rate is set to 60 Hz. A wooden fitting around the force transducer is integrated into the flume to avoid flow
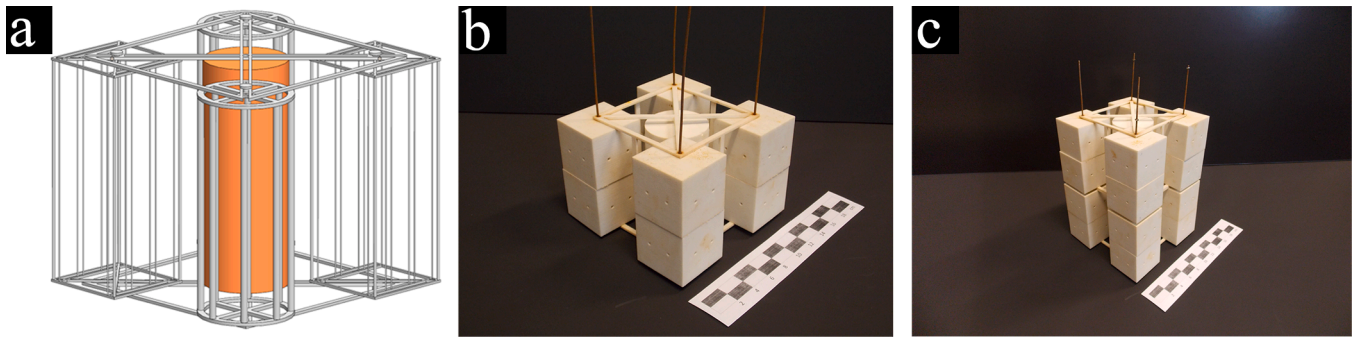
Fig. 3. Shellfish Tower during design stage [Heasman et al, 2020] (same issue) with buoyancy tank in orange and four sub-units (cuboid and cylindrical) attached (a) as well as the single (b) and double (c) model with cylindrical sub-units used in the physical experiments.

separation induced turbulences. The fitting is 0.05 m high, 2 m wide and 3 m long. The ramps at both ends are 0.3 m long. The force sensor is embedded into the fitting 2 m behind the fittings' frontal edge and firmly attached with four screws. Its cable is passed below the fitting to one side of the flume to avoid flow separation. Flow velocity profiles are measured 1 m behind the fittings' frontal edge with a hydrometric vane (Nixon Streamflo Velocity 403, Nixon Flowmeters Ltd. Leckhampton, Cheltenham, UK) in 0.05 m spacing over the whole water depth for each current velocity. The velocimeter has a range of 5–150 cm/s and an accuracy of $\pm 2\%$ of true velocity. Looking into the current direction, the model is situated 1 m behind the vane, so an undisturbed velocity profile is measured. At each location, three 10 s mean values were measured for each of the current velocities. The tilting angle of the cages for each flow velocity is determined via post-processing of pictures taken from a side view with a digital compact camera (Coolpix L810, Nikon, Tokyo, Japan). Four coloured markers, forming a virtual rectangle with 0.95 m length and 0.39 m height around the set-up and one additional marker at the lower end of the model as well as at the mooring point, were used to reference the models' position in the flume. Fig. 2 shows the instrumentation used and the placement of all components in the flume. For each of the tested model variants the mooring force as well as the inclination angle in five different current velocities were determined. At least four repetitions per test are conducted to account for variability. In total 40 tests were conducted. The tested velocities are 0.1 m/s, 0.2 m/s, 0.3 m/s, 0.4 m/s and 0.5 m/s measured at the water level where the model is situated. These current velocities correspond to velocities from 0.45 m/s to 2.24 m/s in prototype scale, which is slightly above the recorded current velocities at the prototype site. The larger range of velocities was however chosen as to inform the designers about the maximum deflection of the cage system.

The data was detrended, filtered and any offset was removed. A 4th order, low-pass Butterworth filter with a cut-off frequency of 3 Hz was used. The maximum line tension may be considered as a combination of static and dynamic load. The static loads, i.e. pretension in the mooring line is a constant force acting in z-direction and can be determined by subtracting the inertial force F_G from the buoyant force F_A:

$$F_{Pre} = F_A - F_G = V\rho g - mg \qquad (1)$$

with $\rho = 1000$ kg/m^3 the density of water, $g = 9.81$ m/s^2 the gravitational force, V the in-air volume of the submerged elements and m as the mass of the structure. The pretension for the different tested structure variants was calculated accordingly and listed in Table 1. The pretension, or static load level, was added to the force in z-direction. The maximum and minimum dynamic loads are defined as peak tension increases or decreases from the static tension load level. Dynamic loads were generated by the longitudinal and horizontal oscillations at the end of the line where the cage is located. As the structure is using a single mooring, the forces are combined into a magnitude force by the following Eq. (2):

$$F_{Magnitude} = \sqrt{F_x^2 + F_y^2 + F_z^2} \qquad (2)$$

with F_x, F_y and F_z being the force in x-, y-, and z-directions, respectively.

Fig. 4 shows the measured flow velocities in comparison to the theoretical logarithmic velocity profile and schematically represents the inclination angle and the resulting position and orientation of the model in the current. The distance to the mooring point x as well as the water height h are normalized with the model structure's diameter, D. To determine the location of the structure, the camera images of each measurement were evaluated automatically using a MATLAB code (Stolle et al., 2017). The markers at the mooring point and the bottom of the model were used to determine the pixel coordinates and therefore the inclination angle γ of the mooring. The current-induced angle α describes the model orientation in relation to the mooring line, which is right-angled in calm water without current and becomes smaller as the current speed and inclination angle increases. The angle β corresponds to the model orientation to the bottom of the flume and is used to identify the characteristic height h_{char}, which represents the vertical distance of the frontal area of the structure encountering the flow. An angle β of 45° leads to the highest forces, since the area exposed to the flow becomes the largest. Thus, it was possible to determine the velocity acting at the respective depth from interpolation between measured values and theory.

Any object in a fluid environment experiences drag, which is the net force due to pressure and shear stress forces acting on the object surface in the flow direction. The drag coefficient is a dimensionless number that describes this resistance with all dependencies of shape and inclination in steady flow conditions and is widely used for research in the field of aquaculture systems (James and O'Donncha, 2019, Zhan et al., 2006, Strand and Volent, 2013). The resulting drag coefficients of this study are calculated as:

$$C_D = \frac{2 * F_{Horizontal}}{\rho u^2 A} \qquad (3)$$

where $F_{Horizontal}$ is the resulting horizontal force acting on the structure, ρ is water density, u is the specific current velocity acting at the water depth where the model is located and $A = D * h_{char}$ is the referential area consisting of the diameter D and the characteristic height of the structure h_{char}. The drag coefficient is related to the Reynolds number Re, expressed by:

$$Re = \frac{u * D_i}{\nu} \qquad (4)$$

where u is the horizontal velocity of the current, D_i is the characteristic diameter of the model and ν is the kinematic viscosity of the water.
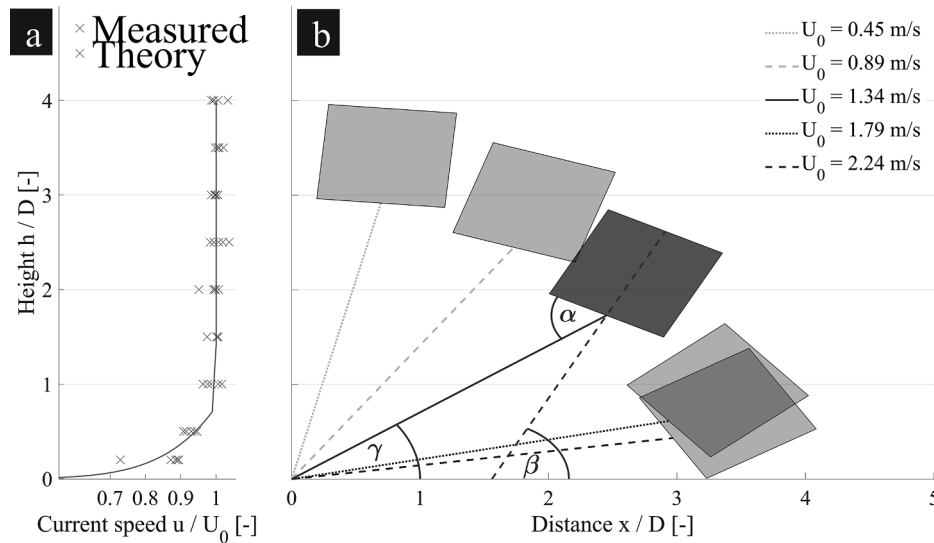
Fig. 4. Normalized velocity u / U0 over normalized height h / D for all measurements compared to theoretical power law velocity profile (a) as well as mooring inclination and indication of different responses for increasing current velocities with γ the deflection angle, α the angle between structure and mooring and β as the resulting angle to the flume bottom (b).

2.3. Wave tests

Experiments in the 3D-wave and current basin were carried out to quantify the forces exerted on the system by both waves and currents. The tests were conducted at a water depth of 1 m corresponding to 45 m water depth in nature. This depth was chosen because it is close to 45 m, the water depth at one of the prototype test-sites. The distance between model and still water surface was 0.01 m. The experimental setup is shown in Fig. 2. The model was moored to the same three-axis-force-transducer used in the current flume tests and was positioned in the middle of the basin. Here, the x-direction represents a movement from the point of origin in the direction of wave propagation; the y-direction corresponds to a movement from the point of origin in the direction of the current flow, while the z-direction is described by a movement from the point of origin towards the top of the basin. The free surface water elevation during wave tests was recorded using an ultra-sonic sensor, USS 20,130, with the corresponding controller ULS 40-D (General Acoustics, 24,106 Kiel, Germany). The accuracy of the sensor is within 0.36 mm. The sampling rate of force transducer and ultra-sonic sensor was set to 100 Hz during data acquisition. Wave and current tests, as well as combinations, were carried out with variations of the parameters: wave height, wave period and current velocity, as well as the model parameters. Wave tests were conducted for propagation angles of 75°, 90° and 105°, with 90° being an orthogonal wave propagation direction regarding the model unit. The models were tested in three current velocities of 0 m/s, 0.34 m/s and 0.46 m/s measured 0.1 m below the water surface at the model's position. These velocities correspond to 0.0 m/s, 1.5 m/s and 2.2 m/s at the prototype scale. The tests without current were only carried out for 90° wave direction, as the results for the single moored system would not change for oblique wave angles. Overall, 112 tests were conducted. The wave kinematics were selected based on the wave regime of possible prototype locations. These sites had wave heights ranging from 1.6 to 5.0 m with periods between 5 to 14 s. Froude similarity with the scaling factor of 20 is applied and the corresponding data is shown in Table 2.

The data was analysed wave by wave, using a time-domain approach, and by selecting relevant data through windowing (period between starting and stopping in time). The starting point for the identification of relevant data was set to when the measured wave height approached more than three-quarters of the set wave height. The stopping point was determined as the time step after the last wave

Table 2
Froude Scaling 1:20 of the waves created in the 3D-wave and current basin during the testing of the *Shellfish Tower*.

Wave ID	Original Wave 1:1		Froude Wave 1:20			
	Wave Height [m]	Wave Period T [s]	Wave Height [m]	Wave Period T [s]	Wavelength L [m]	Wave Steepness H/L
1	1.6	5	0.08	1.12	1.93	0.039
2	3	8	0.15	1.79	4.41	0.034
3	4	10	0.20	2.24	6.10	0.033
4	5	14	0.25	3.13	9.28	0.027

reached more than three-quarters of the set wave height. Each wave between these points was identified individually via zero-down crossing and the wave height, period and length were determined. The synchronized data of the force transducer were similarly divided into the x-, y- and z-force components for each wave. An example of the analysis period, along with time-histories of surface elevation, and three force components is displayed in Fig. 5 for the single configuration, no current and a wave height of 4.0 m and a wave period of 10 s.

For each wave, the dynamic forces were combined with the static pretension into the magnitude force (cp. Eq. 2). The identified waves were analysed by calculating the empirical cumulative distribution function (ECDF) of the magnitude forces. This function is described as (Lawless, 2011):

$$\widehat{E}_n(x) = \frac{1}{n} \sum_{i=1}^{n} 1(X_i \le x) \tag{5}$$

with n being the number of data points in the time series of the waves and x the value of the magnitude force. $\widehat{E}_n(x)$ is a monotonic, nondecreasing, right-continuous function with left-hand limits and a finite number of entries. The function describes the force distribution for the different test conditions over a cumulative probability and is normalized over the maximum occurring force of every test. The shape of the function indicates the distribution of the overall load, i.e. a sharp incline of the curve points to spikes in the force time series. By evaluating the shape of the function, a discussion of the load evolution of the *Shellfish Tower* was conducted. For example, the load distribution and ECDFs for the single configuration of the model for all three current velocities and a wave with a height of 4.0 m and a period of 10 s (in prototype scale)
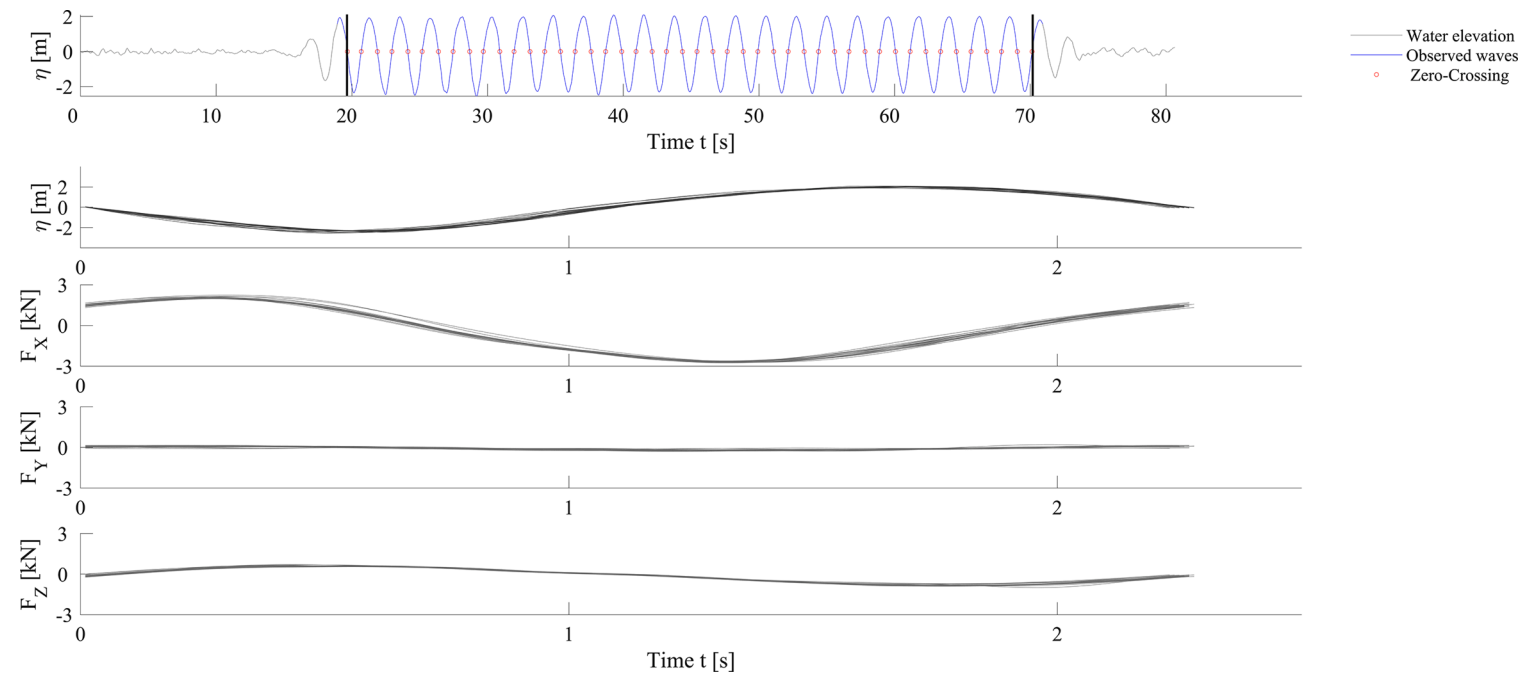
Fig. 5. Overall water surface elevation of test wave 3 (H = 0.2 m, T = 2.24 s) with starting and stopping points for zero-crossing analysis and isolated surface elevations displayed alongside corresponding force components in x-, y- and z-direction excluding pretension.
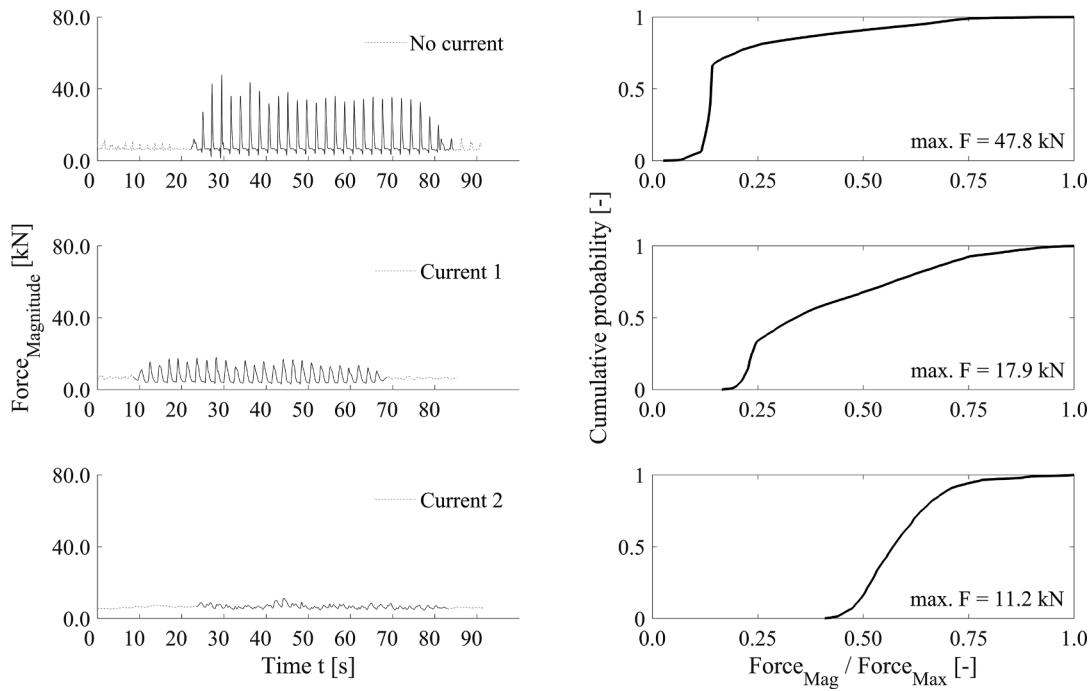
Fig. 6. Force evaluation based on the single configuration of the model for all three current velocities and a wave height of 4.0 m and wave period of 10 s (in prototype scale) propagating from 90° Empirical cumulative distribution function for each case on the right.

Table 3

: Reynolds Number *Re*, horizontal mean force $F_{Horizontal}$ and drag coefficient C_D for the single and double configuration of the *Shellfish Tower* for the tested current velocities u_c.

		Single	Double
Current 1	*Re*	$0.80 \cdot 10^6$	$0.95 \cdot 10^6$
	$F_{Horizontal}$	1.41 – 1.53	3.00 – 3.42
	C_D	2.21 -2.40	2.18 - 2.53
Current 2	*Re*	$1.95 \cdot 10^6$	$1.89 \cdot 10^6$
	$F_{Horizontal}$	4.02 – 4.77	7.49 - 9.24
	C_D	1.10 - 1.35	1.43 - 1.79
Current 3	*Re*	$2.77 \cdot 10^6$	$2.71 \cdot 10^6$
	$F_{Horizontal}$	5.68 - 6.08	11.20 - 11.72
	C_D	0.89 – 0.95	1.06 - 1.17
Current 4	*Re*	$3.66 \cdot 10^6$	$3.56 \cdot 10^6$
	$F_{Horizontal}$	5.80 - 6.60	10.91 - 12.94
	C_D	0.58 - 0.65	0.64 - 0.77
Current 5	*Re*	$4.44 \cdot 10^6$	$4.41 \cdot 10^6$
	$F_{Horizontal}$	6.05 - 6.40	11.51 - 13.01
	C_D	0.41 - 0.46	0.46 - 0.53

propagating from 90° are shown in Fig. 6. The time-histories of the magnitude force are displayed for the different current velocities on the left and the ECDFs are displayed on the right.

3. Results

3.1. Current tests

This section outlines the results of the current induced forces and resulting drag coefficients based on the analysis described in chapter 2.2. In Table 3, the Reynolds numbers, measured horizontal forces and the calculated drag coefficients for the single and double configuration of the Shellfish Tower for the tested current velocities are shown. The maximum mooring forces for the single and double configuration are between 6.05 to 6.4 kN and 11.51 to 13.1 kN, respectively. Generally,

the forces increase with the current velocity. With a constant model diameter across both height configurations, the current velocity is the only variable influencing the Reynolds number, which ranges from $Re = 0.8$ to $4.4 * 10^6$ for the conducted tests. Fig. 7 shows the drag coefficient over the Reynolds number. The determined drag coefficients range from $C_D= 0.5$ to 2.5 for $Re = 0.8$ to $4.4 * 10^6$. The drag increase of the double configuration visible in Table 3 as well as Fig. 7 is due to the larger surface area in comparison to the single configuration. Fig. 8 shows the drag coefficients with the corresponding deflection angles of the mooring ranging from 12° to 84° for the same Reynolds numbers. The dark coloured band in Fig. 7 and Fig. 8 corresponds to conditions typically seen in the Bay of Plenty, the application area of the prototype *Shellfish Tower*, with drag coefficients ranging between $C_D = 1.7$ to 3.1 and inclination angles between 0 to 28° A 2nd order nonlinear regression analysis was performed to establish a fit through the data points and allow for the resulting drag coefficients to be determined for specific sites using the Reynolds number. This is represented by the dashed lines in Fig. 7 and Fig. 8, where the quadratic regression curves in the form $p_1x^2 + p_2 x + p_3$ from the drag coefficient C_D, in order to illustrate the dependency on the Reynolds number and the deflection angle, respectively.

3.2. Wave tests – maximum and median forces

Based on the analysis described in chapter 2.3 the median and maximum forces for the single and double *Shellfish Tower* are shown in Table 4. The median was chosen as a descriptor because it is robust against outlying data. Results for all tested waves (cp. Table 2), current velocities, and wave directions are given in Table 4. A large difference between median and maximum load is shown in the results. The forces exerted on the mooring are highly sensitive to the current while model height, wave dynamics and directions are of lesser influence. The maximum forces for the single and double configuration are between 7 - 48 kN and 20 - 89 kN. The median forces range from 6 to 8 kN and 7 to 14 kN, respectively. The large difference between the median and maximum value, visible for both configurations, can be attributed to the varying input parameters, which affect the motion of the *Shellfish Tower*
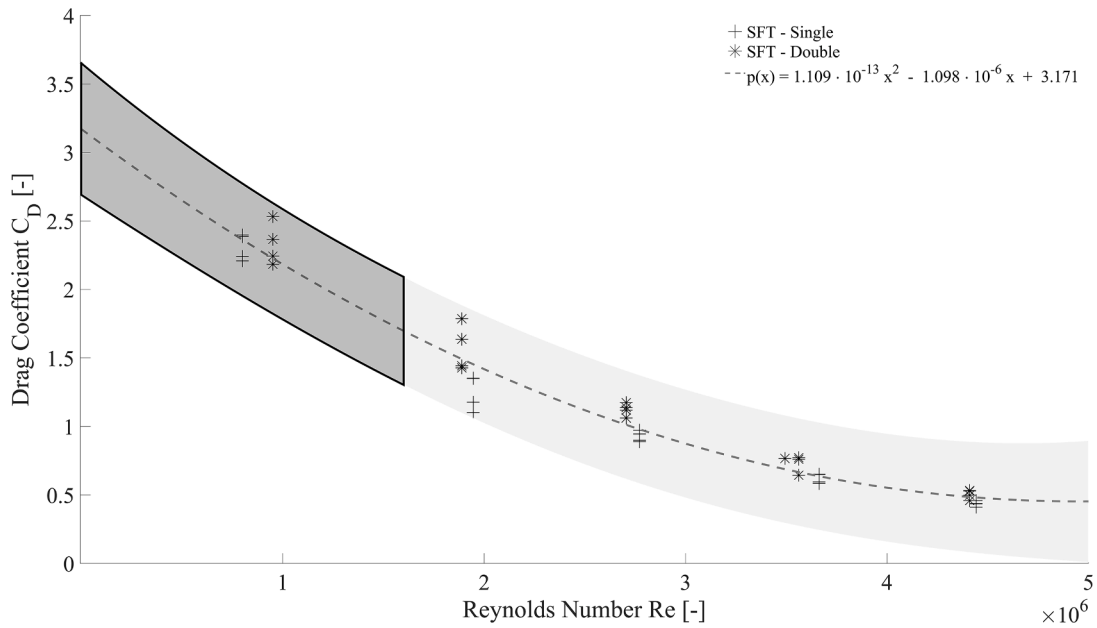
Fig. 7. Current induced drag Coefficient C_D over Reynolds Number Re of all test cases for the single and double configuration of the Shellfish Tower with nonlinear fit and indication of expected Re-Numbers in the Bay of Plenty.
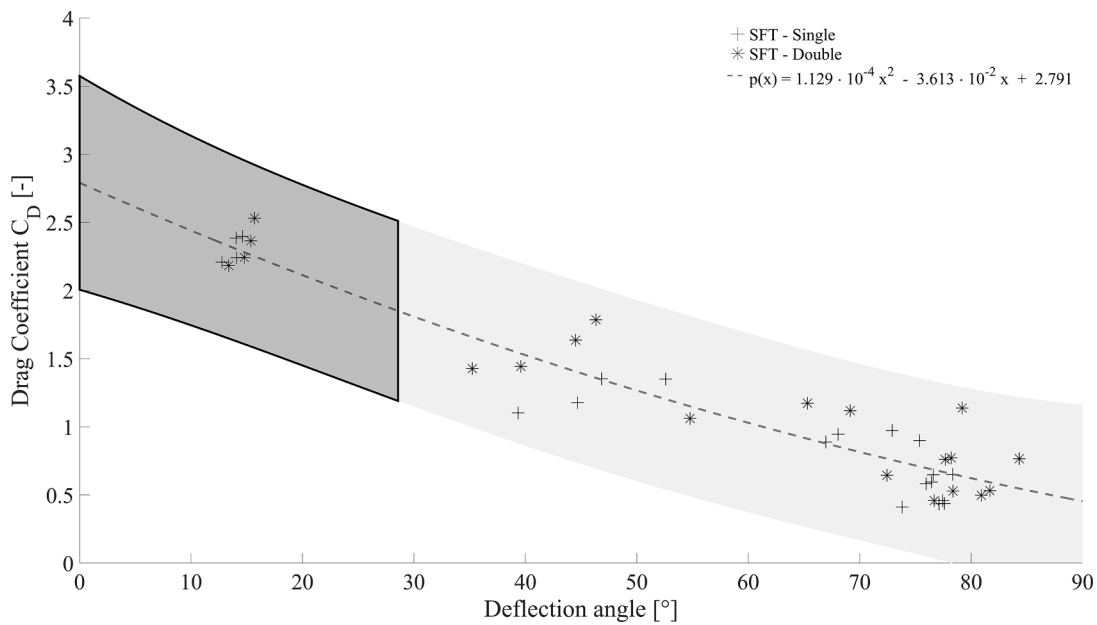

Fig. 8. Current induced drag coefficient C_D over the deflection angle $90° - \gamma$ of all test cases for the single and double configuration of the Shellfish Tower with nonlinear fit and indication of expected deflection angle in the Bay of Plenty.

system. The current velocity influences the position of the *Shellfish Tower* in the water column as well as the median force level. Due to the longer mooring line, the inclination angle γ of the system is reduced compared to the current tests in chapter 3.1. Accurate measurements of the deflection angle were not feasible due to the 3D-nature of the experiments and so deflection angles of up to approximately 45° were estimated visually. The largest occurring forces for the single configuration are 47.8 kN and the peak force observed for the double configuration a peak force is 89.3 kN (median values were 6.6 kN and 13.3 kN respectively). The maxima for both configurations are recorded during tests with no current, wave heights of 4.0 m and wave periods of 10 s. Increasing the current velocity causes the maximum forces to decrease, e.g. the maximum force observed on the single configuration in 2.2 m/s

current is 77% less than when no current is applied. The median force decreases by 3% and similar trends are seen for the double configuration. To determine the influence of the current on the force evolution the median and maximum values for each wave-current setup are further analysed. This enables a more in-depth look at the importance of the current in regard to the forces on the system as well as the wave dynamics. Fig. 9 shows the median and maximum forces over the wave steepness for all directions, current velocities and both the single and double configuration of the *Shellfish Tower*. The median values are nearly constant for both single and double configurations (6 to 8 kN and 7 to 14 kN, respectively) while the maximum values vary with wave dynamics as well as currents. Without the presence of a current, the maximum forces increase with the wave steepness, while with a current

Table 4
Maximum F_{max} and median $\bar{F}$ forces [in kN] for the single and double configuration of the *Shellfish Tower* shown for the tested current velocities u_{c1-3} and waves 1 - 4.

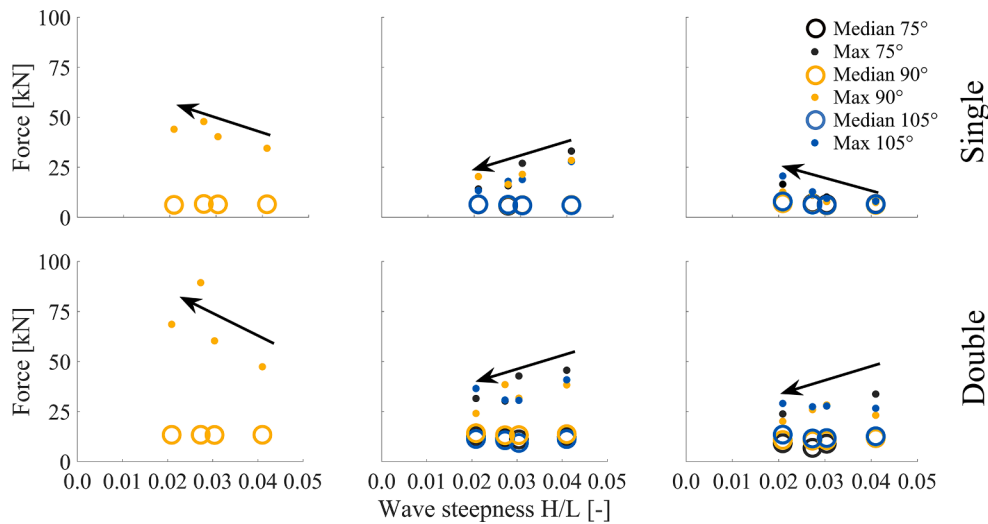| | | Current velocity | | | | | | | | | | |
| | | u_{c1} = 0.0 m/s | | | | u_{c2} = 1.5 m/s | | | | u_{c3} = 2.2 m/s | | | |
| | | Single | | Double | | Single | | Double | | Single | | Double | |
		F_{max}	$\bar{F}$	F_{max}	$\bar{F}$	F_{max}	$\bar{F}$	F_{max}	$\bar{F}$	F_{max}	$\bar{F}$	F_{max}	$\bar{F}$
Wave 1	75°	34.4	6.5	47.3	13.3	33.0	6.1	45.6	12.2	8.2	6.6	33.7	12.0
	90°					27.8	6.1	38.2	11.2	7.4	6.2	23.1	11.6
	105°					28.4	6.5	40.8	13.6	8.0	6.5	26.6	12.6
Wave 2	75°	40.2	6.4	60.3	13.2	26.9	6.0	42.7	11.0	10.1	6.5	27.7	8.9
	90°					18.8	5.9	31.6	9.3	7.8	5.9	28.2	10.5
	105°					21.4	6.0	30.5	13.2	9.4	6.0	27.7	11.7
Wave 3	75°	47.8	6.6	89.3	13.3	17.7	5.8	30.2	11.7	11.0	6.8	25.9	6.8
	90°					17.9	6.2	38.4	10.6	11.2	6.4	25.9	10.4
	105°					16.4	6.3	30.7	13.1	12.7	6.3	27.3	11.5
Wave 4	75°	43.9	6.2	68.5	13.3	14.1	6.4	31.5	12.8	16.5	7.1	23.7	9.1
	90°					13.3	6.4	24.0	11.2	12.6	7.0	20.0	10.7
	105°					20.3	7.9	36.5	14.1	20.6	7.9	29.0	13.4

Fig. 9. Median and maximum forces over the wave steepness for all directions, current velocities and both the single and double configuration of the Shellfish Tower. Arrows indicate the approximated rise or fall of the forces in regard to the wave steepness.
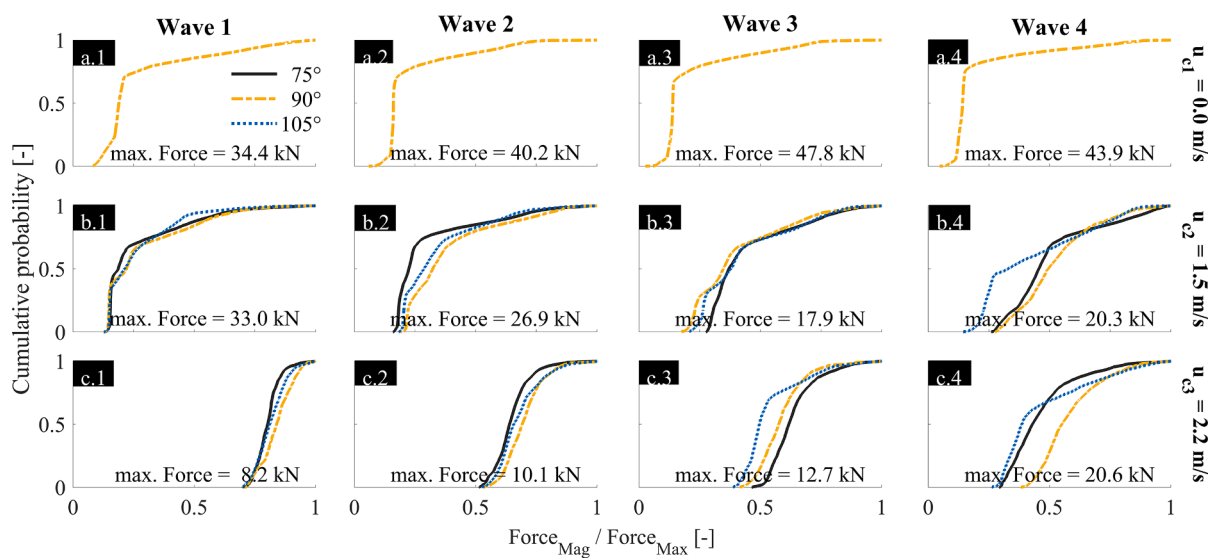

Fig. 10. Empirical cumulative distribution functions of all test cases for the single configuration of the Shellfish Tower separated by the tested current velocity uc1 = 0.0 m/s, uc2 = 1.5 m/s and uc3 = 2.2 m/s as well as by wave 1 (H = 1.6 m, T = 5 s), wave 2 (H = 3.0 m, T = 8.0 s), wave 3 (H = 4.0 m, T = 10.0 s) and wave 4 (H =5.0 m, T = 14 s).
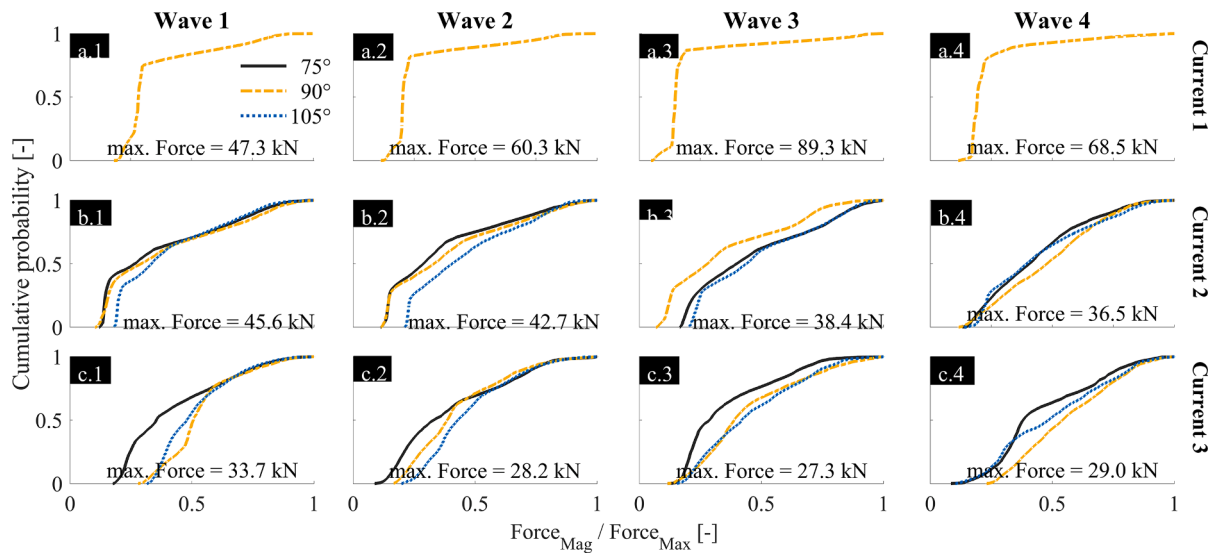
Fig. 11. Empirical cumulative distribution functions of all test cases for the double configuration of the Shellfish Tower separated by the tested current velocity uc1 = 0.0 m/s, uc2 = 1.5 m/s and uc3 = 2.2 m/s as well as by wave 1 (H = 1.6 m, T = 5 s), wave 2 (H = 3.0 m, T = 8.0 s), wave 3 (H = 4.0 m, T = 10.0 s) and wave 4 (H =5.0 m, T = 14 s).

active an opposite trend can be observed. Arrows indicate this approximated rise or fall of the forces in regard to the wave steepness.

3.3. Wave tests – ECDF

One of the objectives of this work is to evaluate the influence of current and waves in an open ocean environment. By concentrating on the discrepancy between the high maximum and significantly lower median loads, a better understanding of the characteristics of the *Shellfish Tower* is gained. Figs. 10 & 11 show empirical cumulative distribution functions (ECDFs) for the single and double configurations, respectively. Here, the ECDFs are displayed in twelve subpanels (a.1 – c.4) with differing waves (columns) and current velocities (rows). The ECDFs of the varying wave directions are plotted together as the influence of wave direction was shown to be of minor relevance. Different characteristics of the ECDFs are identified for both the single and double configuration with the current as the influencing parameter. When there is no current (cp. a.1 – a.4 in Fig. 10), the probability of occurrence for low to medium forces (2.4 – 11.9 kN) is about 70%, shown by the direct and sharp inclination of the curve. As the cumulative probability increases from 0 to 70% the normalized force only increases from the

minimum of 0.08 to 0.18. These low to medium values represent the quasi-static tension within the mooring line. For cumulative probability >70%, the gradient changes drastically as the normalized force levels out towards the maximum value of one. High peak loads in the mooring system of the *Shellfish Tower* give reason for this sudden change in gradient. The steep gradient, visible for a cumulative probability higher than 95%, is especially indicative of these events. Snap loads cause these high-energy events, as the system falls slack after the previous higher wave load in the absence of a current. All varying waves without current show the same characteristic. However, an increase in wave height and wave period also leads to an increase in maximum forces and a steeper gradient is indicative of the snap loads. The highest maximum forces can thus be attributed to the snap load events. With a 1.5 m/s current present, the overall characteristics of the probability distribution differ, as the abrupt change in gradient is less prominent. With increasing periods as well as amplitudes, the shape of the ECDF changes to a more linear distribution (cp. b.3 & b.4 in Fig. 10), which indicates a more cyclic force evolution and the absence of snap loads. These forces are representative of the dynamic loads acting on the system without the influence of snap loads. Another change in the characteristics can be observed for the single configuration and an increased current velocity
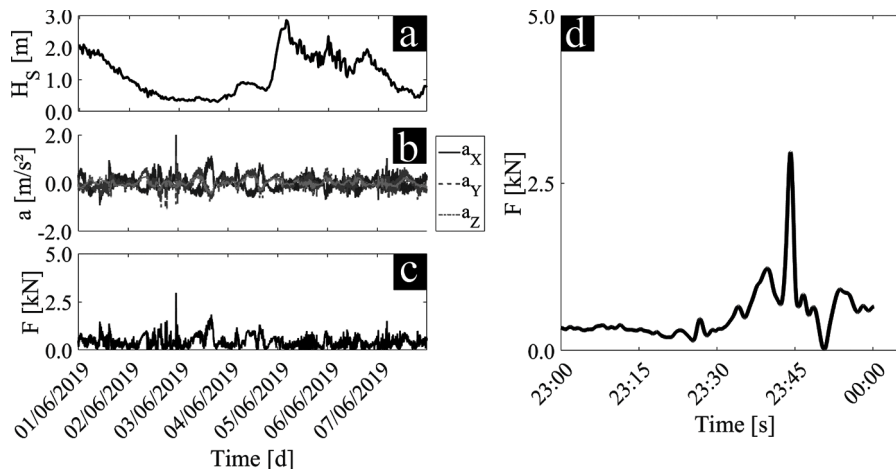

Fig. 12. Significant wave height (a), acceleration of the Shellfish Tower (b) and associated forces due to acceleration (c) with snapping loads (d) during prototype deployment in the Bay of Plenty, New Zealand.

of 2.2 m/s. The maximum forces are low with a small, normalized force range, which indicates overall low forces. This is especially visible for waves with low periods (cp. c.1 in Fig. 10). This distribution can be attributed to the submergence of the *Shellfish Tower* due to the increased current velocity. The small range of normalised forces covered is another indicator for the submergence, as the low forces are caused by the dynamic tension induced through small orbital motions. The results for the double configuration (see Fig. 11) differ regarding the maximum values but show similar characteristics for the probabilistic load distribution. When there is no current, the same observations as for the single configuration apply as the prominent snap loads lead to the highest maximum forces. For a current velocity of 1.5 m/s as well as 2.2 m/s the loads are reduced as the snap events are not as prominent due to pretension in the mooring line caused by the current, as well as a submergence of the structure. A near linear distribution of the ECDF can be found for all remaining cases (cp. b.1 – c.4 in Fig. 11). The presented results in Fig. 10 and Fig. 11 allow for a probabilistic determination of the design load on the mooring system of the *Shellfish Tower*. Provided that the metocean conditions of a potential site are available, the data can be used for an initial approximation of the possible loads.

3.4. Prototype tests

These snap load events were also observed during the real-world deployment of the Shellfish Tower prototype in the Bay of Plenty, New Zealand (cp. Fig. 12d). The sampling frequencies (30 minute) of the load cell attached to the prototype mooring and the wave buoy moored nearby were insufficient to detect snap loads. However, an accelerometer (OpenTag Motion Datalogger, Loggerhead Instruments, Sarasota, USA) with a sampling frequency of 50 Hz was attached to the steel frame of the Shellfish Tower. Acceleration data recorded between 01.06.2019 and 07.06.2019 was used in combination with the original and hydrodynamically added mass of the prototype to calculate the forces on the Shellfish Tower. Thus, the forces of acting on the Shellfish Tower prototype (cp. Fig. 12c) are displayed as:

$$F = m * a_{mag} \qquad (6)$$

With m being the original and hydrodynamically added mass of the prototype and a_{mag} the combined observed acceleration in x-, y- and z-direction (cp. Fig. 12b). The added mass was approximated for a cylinder with the same height and diameter of the hexagonal prototype according to:

$$m_a = \rho \pi R^2 L \qquad (7)$$

Despite the high buoyancy of the prototype supported by a buoy at sea level, snap events could be observed where the induced peak loads on the system are multiple orders higher than the average loads. The occurrence of snap loads does not correlate with the significant wave height due to the averaged nature of said data set. However, the accelerometer data shows that single wave events can cause snap loads in the system. Similar to the model tested in the wave basin the prototype is pulled upward when the crest of a wave is at the prototype's location and a cyclic in- and decrease in the resultant force (quasi-static load) is visible. Single wave action can cause the prototype to experience snap loads, as can be seen in Fig. 12. The following submergence of the prototype can also be observed by the reduction in force, thereafter. This confirms the observations made during the model tests and stresses the need for operational and technical measures to reduce snap loads, as these could adversely affect the longevity of the Shellfish Tower system. Further information regarding the deployment is given in the companion paper Heasman et al. (2021) (same issue)

4. Discussion

4.1. Current tests

The current tests showed that the pretension generated by the buoyancy has a decisive influence on the determined forces (cp. Table 1). The greater the buoyancy of the body, the lower the mooring inclination, which reduces the horizontally acting forces on the structure and increases the vertically acting forces. Together with the results of the wave tests (cp. chapter 3.2), the authors would advise for excess buoyancy to be considered during the installation of submerged aquaculture systems. Furthermore, the results showed that the drag coefficients of the single models are all slightly lower than those of the double model configuration, due to the influence of the aspect ratio $\left(\frac{h_{char}}{D}\right)$ on the structure's drag. The height h_{char} of the double configuration and therefore the aspect ratio is twice as large while the end tip vortex effect on the wake above and below the structure remains similar (Potts et al., 2019). The increasing flow velocities are the driving factors for the decreasing drag values, as they are quadratically included by the kinetic energy component for the calculation of the drag coefficient (cp. Eq. 3). The resulting angle β and therefore the frontal area of the structure exposed to the flow affects the drag coefficients as well, but to a lesser extent than the current speed. With increasing current velocities, the structure tends to tilt further towards the flume bottom and is therefore partly located in the logarithmic boundary layer profile with reduced velocities. This effect occurs at speeds >1.8 m/s and further reduces the drag coefficient. The deflection is strongly dependant on the buoyancy generated by the installed structure. The mass-buoyancy force ratio for the investigated structure is 1.22 (cp. Table 1) and increasing this could reduce the inclination susceptibility of the structure (Lu et al., 2011). The effect the buoyancy force has on the overall system response to waves and currents is equally important for the design and safe deployment.

4.2. Wave tests

The importance of carefully choosing the buoyancy can also be seen in the results from the wave tests as highlighted by the small range of all median values (cp. Table 4). The higher the buoyancy, the higher the static tension and therefore the higher the median load. This can be seen in a comparison between the single and double configurations of the *Shellfish Tower* (cp. Fig. 9), where the median loads are twofold with the doubled buoyancy. The recorded forces are sensitive to wave direction and increase when current and waves are superimposed (wave direction = 105°). The magnitude of this increase depends on wave height and as wave height increases, the effect becomes more pronounced. Evidently, in Fig. 9, without a current, the maximum forces due to snap loads increase with the wave steepness. The steeper waves lead to an increased vertically acceleration of the *Shellfish Tower*, which causes a more rapid onset of snap loads and afterwards the system to fall slack in the absence of a current. The circumstance that high wave steepness causes large structure motion was also observed by Qin et al. (2020). The steeper the wave, the higher the snap loads observed. In the presence of a current, the highest loads coincide with the least steep waves. It can be assumed, that this is due to the pretension in the mooring line applied by the current. The *Shellfish Tower* system is further submerged in the water column and less receptive for snap loads. Steeper waves submerge the system even further. This is why the local wave characteristics have to be closely observed when researching new marine systems. For wave heights of 1.6 m and periods of 5.0 s, 6% increase in median force was observed while wave heights of 5.0 m and 14.0 s period produced an increase of <22%. This increase is due to the current-induced pretension in the mooring as well as the dynamic tension of the larger waves. Divergent currents and waves (wave direction = 75°) had no discernible effect on the median forces. For a wave direction of 75°, the maximum
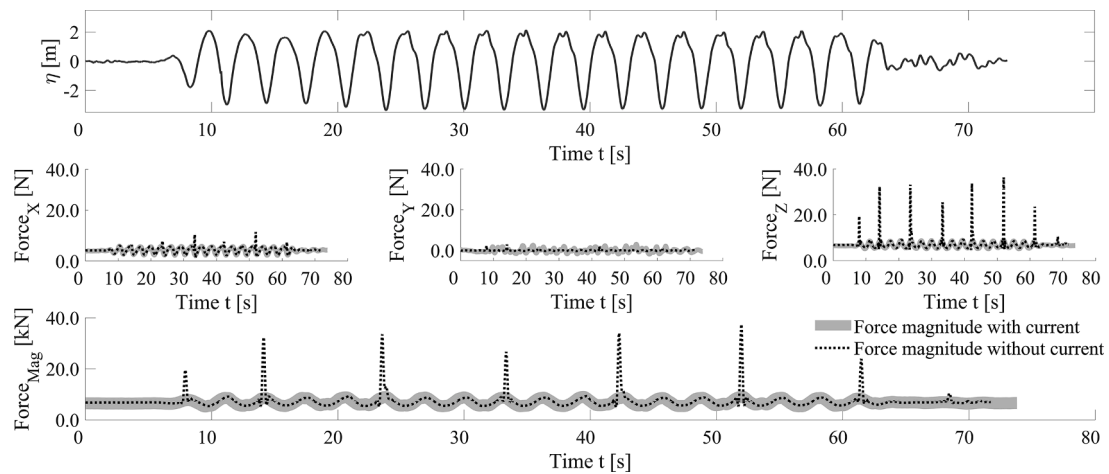
Fig. 13. Comparison of force magnitude for an exemplary case (single configuration, H = 4.0 m, T = 10 s, Dir = 90°) with (uc = 2.2 m/s) in comparison to the no current case (uc = 0.0 m/s) to exemplify occurring snap loads in the Shellfish Tower system. The x-, y- & z-force components forming the magnitude force are displayed.

forces increased due to the slacking of the mooring line, which is caused by the divergent directions of the currents and waves, as well as the orbital motion of the wave, which causes a sudden re-tensioning. This resulted in strong snap loads. This finding was instrumental in the design of the cage system and became design relevant throughout the overall process. The increase in drag from the larger area of the double configuration of the *Shellfish Tower* results in higher forces. An increase in maximum loads by approximately a factor of four can be observed between the different configurations (cp. Table 4). Median loads increase by 215%. Thus, a duplication of the tower section results in a doubling of the median loads, which confirms design assumptions considered for early design stages. However, the four-fold increase in maximum force for an additional cage shows that the motion of the double system under waves and currents needs more investigation, as it has to be accounted for during the mooring design of potential aquaculture farms. This result provides important information to the system designers and indicates that further testing will have to take place when the final system design is to be up scaled for economic or operational.

4.3. Snap loads

The high maximum loads visible in the results (cp. chapter 3.2) of the wave tests are attributed to snap loads. These are impact loads caused by the sudden tensioning of the mooring line after a state of zero tension, which mostly occurs when the mooring system is subjected to motions with large amplitudes. The duration of the snap load is instantaneous, but its amplitude can be many times greater than the maximum dynamic load as can be seen in Fig. 13. Here, the force magnitude for a wave height of 4.0 m and a wave period of 10 s is displayed for two time-histories: (1) with a current velocity of u_c = 2.2 m/s and, (2) without current. A tenfold difference between the force peaks can be observed. The main contributors are the z- and x- component of the force, whereas the y-components have a negligible influence. Without current nor waves present, the *Shellfish Tower* is floating upright, close to the water surface. During current activity, the *Shellfish Tower* is tilted, and the mooring line is pretensioned. Without the presence of waves, only the static tension needs to be considered. When the crest of the wave is at the model's centre location, it is pulled upward, causing a peak in the resultant force shortly before the crest. This describes the normal, quasi-static tension for any moored system in a wave environment. During the following wave trough, the vertical forces of the orbital wave motion push the model downward. It cannot rise to its initial position and is submerged for the next wave and the mooring line falls slack. The next wave crest though causes a rapid re-tensioning and results in the high

snap load. Through the spring-like restoring force in the mooring line, the model is significantly submerged. Here, the exerted wave forces are significantly lower. Only when, as depicted in Fig. 13, the third wave after the snap event propagates towards the model, has the model risen far enough up in the water column for the mooring to fall slack again due to the wave's amplitude. It instantaneously tightens again, resulting in the next snap load. These snap load events were observed for all wave heights and -periods as well as directions. Without the added pretension of the current, these events are especially dominated by high force levels and this yields the highest maximum loads (cp. Table 4). For a current velocity of 1.5 m /s, single snap events could still be detected. No snap load events occurred for a current velocity of 2.2 m/s.

While snap load events are to be avoided, a good understanding of the hydrodynamics and structure's response is crucially important for the design of any structure in open ocean environments. Snap loads are a known problem for the established oil and gas industry and pose a major challenge to robust mooring design for the growing aquaculture industry as was stated in the introduction. To mitigate the risk of snap loads on aquaculture systems such as the *Shellfish Tower* an increase of the safety factor in would minimize the risk of system failure and ensure longevity in high energy, open ocean conditions. A high flotation to mass ratio increases the resistance of the *Shellfish Tower*, or any other floating system, to the downward-orientated component of the orbital wave motion and increases the station-keeping capability. This is a major result of this work, directly feeding back into the design process described in the companion paper Heasman et al. (2021) (same issue). However, if a sufficiently large wave amplitude causes the mooring to slacken, then, as the orbital wave motion induces an upward force on the system, the additional flotation will combine with the water flow, increasing the speed of the *Shellfish Tower* rising in the water column, resulting in higher snap forces. Conversely, a lower flotation to mass ratio (as a result of less flotation or higher shellfish biomass) will result in the mooring falling slack more easily as the *Shellfish Tower* is driven down with the orbital wave motion. As the wave progresses and the downward motion changes to an upward motion, the speed of the *Shellfish Tower* will be reduced as the combination of flotation force and water flow are not as great, reducing the snap force. Similarly, the results from the model test in the current flume suggest that with an increase in buoyancy the inclination of the mooring becomes smaller while the pretension increases. Thereby the vertical force component is continuously increasing compared to the horizontal force component, which also reduces the resulting angle α of the *Shellfish Tower* to the connection point of the mooring. In the case of oyster farming, while periodic movement of the oysters within the oyster basket prevents the

oyster shells from growing and adhering together and increases the shell thickness and strength, the movement caused by the snap load event may prove to be disruptive to the grow-out of the product, with shell damage and loss of the oysters. The disadvantages of snap loads are that the shell of the oysters could be damaged by the abrupt stopping of the *Shellfish Tower* units, which leads to abnormal abrasion of the shell. In particular, the newly formed distal part of the shell could break off when the oysters are knocked together (Newkirk et al., 1995, Pogoda et al., 2011). The external appearance of the oyster shell plays an important role in the "half-shell-market" (Mueller Loose et al., 2013) for the consumer (Matthiessen, 2001), so any damage will reduce the value of the oyster. The same applies to the culture of mussels (e.g. green-lipped mussels or Blue/Mediterranean mussels) as they could be shaken off their substrates. Although the choice of the longline in its surface condition could improve the adhesion of byssus plaques (Brenner and Buck, 2010, Babarro and Carrington, 2013), the risk of biomass reduction through snap events can have both ecological and economic consequences. With some macroalgae (e.g. family *Laminariales*) a tip loss occurs seasonally. This could be increased by snap events, which could lead to a lower biomass at harvest. The *Shellfish Tower* could be repositioned deeper in the water column to avoid the damages caused by the snap event. However, by placing the system in deeper water it may be positioning the system below the optimal availability of phytoplankton and organic particulate matter on which the shellfish feed. Prior to the *Shellfish Tower* being deployed, the site-specific factors should always be examined. If the phytoplankton density and quality allow, the *Shellfish Tower* could be installed deeper in the water column where the orbital wave is smaller leading to less forces and therefore the snap load phenomenon is low or non-existent. The importance to submerge the system during storm events has been highlighted by Kim et al. (2014). If this is not possible then technical improvements should be considered that prevent or greatly reduce snap load events. These could include the installation of shock absorbing elements, such as spring-like elements, rubber structures or other components that buffer the abrupt force on the *Shellfish Tower* (Gordelier et al., 2015). Alternatively, floating breakwaters could be installed. An investigation by Dong et al. (2008) showed that these may be adopted for aquaculture engineering in deep-water regions to provide effective protection for aquaculture systems.

5. Conclusion

This study assessed the feasibility and functionality of an aquaculture system usable for the collection and cultivation of mussel spat as well as grow out of oysters, scallops and seaweed in marine environments using comprehensive tests conducted under laboratory conditions. A submersible cage system was tested at a 1:20 scale at the Ludwig-Franzius-Institute 3D-wave and current basin and at the inclinable current flume of the Leichtweiß-Institute in open ocean conditions with wave heights up to 5.0 m, wave periods up to 14 s and current velocities up to 2.2 m/s in prototype scale. The main conclusions of this study are that:

- A detailed examination of the mooring line tensions, current velocities, and inclination angle from the experiments in the current flume revealed that the drag coefficients decrease with increasing current velocities from C_D=0.5 to 2.5 for *Re*-numbers = 0.8 to 4.4 $*10^6$, while the mooring inclination increases from $12°$ to $84°$.
- The comprehensive examination of the mooring line tensions recorded in the wave basin showed that the largest values of snap-induced tension were up to 10 times that of the quasi-static tension. The maximum-recorded tension on the system was 47.8 kN for

the single and 89.3 kN for the double configuration, compared to non-snap tension values, which were in the range of 6 – 10 kN.
- Without the added pretension of the current snap events are especially force intensive and result in maximum loads. For a current velocity of 1.5 m /s, single snap events could still be detected while no snap load events occurred for a current velocity of 2.2 m/s.
- To avoid an underestimation of the design loads, the authors recommend time-resolved, dynamic modelling of the coupled structure with the moorings to take snap loads and associated high accelerations into account during the design of open ocean aquaculture systems.

The insights gathered in this study, in conjunction with the results of Heasman et al. (2021) (this issue), provide an interdisciplinary approach to the design and evaluation of a novel aquaculture system usable in marine environments. In the light of the increasing demand for marine protein, the results of this study regarding the drag coefficient of the *Shellfish Tower* system and the probabilistic load distribution can be used as a robust estimate for the planning of future farm concepts.

CRediT authorship contribution statement

Jannis Landmann: Conceptualization, Methodology, Writing – original draft, Writing – review & editing. **Lukas Fröhling:** Methodology, Writing – original draft, Writing – review & editing. **Rebekka Gieschen:** Investigation, Writing – review & editing. **Bela H. Buck:** Investigation, Writing – original draft, Writing – review & editing. **Kevin Heasman:** Investigation, Resources, Writing – original draft, Writing – review & editing. **Nicholas Scott:** Investigation, Resources, Writing – review & editing. **Malcolm Smeaton:** Investigation, Resources, Writing – review & editing. **Nils Goseberg:** Conceptualization, Funding acquisition, Writing – review & editing, Supervision. **Arndt Hildebrandt:** Conceptualization, Funding acquisition, Writing – review & editing, Supervision.

Declaration of Competing Interest

The authors declare that they have no known competing financial interests or personal relationships that could have appeared to influence the work reported in this paper.

Acknowledgments

References

FAO, 2020. Fishery Statistical Collections of the Food and Agriculture Organisation of the United Nations (FAO). Dataset on Global Aquaculture Production (online query), Rome.

Dawber, C., N.Z.M.F. Association., 2004. Lines in the water: A History of Greenshell Mussel Farming in New Zealand. River Press, Picton, New Zealand.

Hickman, R.W., 1992. Mussel cultivation: The mussel Mytilus: ecology, physiology, genetics and culture. Development in aquaculture and fisheries science. Dev. Aquacult.Fish Sci 465–510.

Buck, B.H., 2007. Experimental trials on the feasibility of offshore seed production of the mussel Mytilus edulis in the German Bight: Installation, technical requirements and environmental conditions. Helgol. Mar. Res. 61, 87–101. https://doi.org/10.1007/s10152-006-0056-1.

Cheney, D., Langan, R., Heasman, K., Friedman, B., Davis, J., 2010. Shellfish Culture in the Open Ocean: Lessons Learned for Offshore Expansion. Mar. Technol. Soc. J. 44, 55–67.

New Zealand Government, Offshore Marine Farms - Spatial Analysis Solutions, 2017.

New Zealand Government, 2019. Aquaculture Strategy. Wellington.

K. Heasman, N. Scott, J.A. Ericson, D.I. Taylor, B.H. Buck, Extending New Zealand ' s Marine Shellfish Aquaculture Into Exposed Environments – Adapting to Modern Anthropogenic Challenges, 7 (2020) 1–7. https://doi.org/10.3389/fmars.2020.565686.

Heasman, K., Scott, N., Smeaton, M., Goseberg, N., Hildebrandt, A., Vitasovich, P., Elliot, A., Mandeno, M., Buck, B.H., 2021. New system design for the cultivation of extractive species at exposed sites - Part 1: System design, deployment and first response to high-energy environments. Appl. Ocean Res. 110, 102603 https://doi.org/10.1016/j.apor.2021.102603.

Hanson, J.A., 1974. Open Sea Mariculture Perspectives, Problems And Prospects. In: Offshore Technol. Conf., Offshore Technology Conference.

Bugrov, L.Y., Muravev, W.B., Lapshin, O.M., 1994. Alternative using of petroleum-gas structures in the Caspian and Black seas for fish-farming and fishing: real experience and rigs conversion prospects. Bull. Mar. Sci. MAR. SCI. 55.

Buck, B.H., 2004. Farming in a High Energy Environment: Potentials and Constraints of Sustainable Offshore Aquaculture in the German Bight. North Sea), University of Bremen.

Cannon, H.W., 1980. Energy from Open Ocean Kelp Farms. US Government Printing Office.

Goseberg, N., Chambers, M.D., Heasman, K., Fredriksson, D., Fredheim, A., Schlurmann, T., 2017. Technological Approaches to Longline- and Cage-Based Aquaculture in Open Ocean Environments. In: Buck, B.H., Langan, R. (Eds.), Aquac. Perspect. Multi-Use Sites Open Ocean Untapped Potential Mar. Resour. Anthr. SpringerOpen, Cham, pp. 71–95. https://doi.org/10.1007/978-3-319-51159-7.

Dalton, G., Bardócz, T., Blanch, M., Campbell, D., Johnson, K., Lawrence, G., Lilas, T., Friis-Madsen, E., Neumann, F., Nikitas, N., Ortega, S.T., Pletsas, D., Simal, P.D., Sørensen, H.C., Stefanakou, A., Masters, I., 2019. Feasibility of investment in Blue Growth multiple-use of space and multi-use platform projects; results of a novel assessment approach and case studies. Renew. Sustain. Energy Rev. 107, 338–359. https://doi.org/10.1016/j.rser.2019.01.060.

Lagasco, F., Collu, M., Mariotti, A., Safier, E., Arena, F., Atack, T., Brizzi, G., Tett, P., Santoro, A., Bourdier, S., Fernandez, F.S., Muggiasca, S., Larrea, I., 2019. DEMONSTRATION OF A MULTI-PURPOSE PLATFORM FOR THE BLUE GROWTH. In: Proc. ASME 2019 38h Int. Conf. Ocean. Offshore Arct. Eng, pp. 1–10.

Buck, B.H., Langan, R., 2017. Aquaculture Perspective of Multi-Use Sites in the Open Ocean - The Untapped Potential for Marine Resources in the Anthropocene. SpringerOpen. https://doi.org/10.1007/978-3-319-51159-7.

Kim, T., Lee, J., Fredriksson, D.W., DeCew, J., Drach, A., Moon, K., 2014. Engineering analysis of a submersible abalone aquaculture cage system for deployment in exposed marine environments. Aquac. Eng. 63, 72–88. https://doi.org/10.1016/j.aquaeng.2014.10.006.

Lader, P., Jensen, A., Sveen, J.K., Fredheim, A., Enerhaug, B., Fredriksson, D., 2007. Experimental investigation of wave forces on net structures. Appl. Ocean Res. 29, 112–127. https://doi.org/10.1016/j.apor.2007.10.003.

Bi, C.-W., Zhao, Y.-P., Dong, G.-H., 2020a. Experimental study on the effects of farmed fish on the hydrodynamic characteristics of the net cage. Aquaculture 524, 735239. https://doi.org/10.1016/j.aquaculture.2020.735239.

Benetti, D.D., Benetti, G.I., Rivera, J.A., Sardenberg, B., O'Hanlon, B., 2010. Site selection criteria for open ocean aquaculture. Mar. Technol. Soc. J. 44, 22–35.

Hildebrandt, A., Landmann, J., Ongsiek, T., Goseberg, N., 2018. Drag coefficients of vertically-mounted full-scale blue mussel dropper lines. In: Proc. Int. Conf. Offshore Mech. Arct. Eng. - OMAE. https://doi.org/10.1115/OMAE201878534.

Plew, D.R., Enright, M.P., Nokes, R.I., Dumas, J.K., 2009. Effect of mussel bio-pumping on the drag on and flow around a mussel crop rope. Aquac. Eng. 40, 55–61. https://doi.org/10.1016/j.aquaeng.2008.12.003.

Gagnon, M., 2019. Self-organization and mechanical properties of mussel culture suspensions: A critical review. Aquac. Eng. 87, 102024 https://doi.org/10.1016/j.aquaeng.2019.102024.

Landmann, J., Ongsiek, T., Goseberg, N., Heasman, K., Buck, B.H.B.H., Paffenholz, J.-A.J.-A., Hildebrandt, A., 2019. Physical Modelling of Blue Mussel Dropper Lines for the Development of Surrogates and Hydrodynamic Coefficients. J. Mar. Sci. Eng. 7, 65. https://doi.org/10.3390/jmse7030065.

Gansel, L.C., Plew, D.R., Endresen, P.C., Olsen, A.I., Misimi, E., Guenther, J., Jensen, Ø., 2015. Drag of Clean and Fouled Net Panels–Measurements and Parameterization of Fouling. PLoS One 10, e0131051. https://doi.org/10.1371/journal.pone.0131051.

Irish, J.D., Fredriksson, D.W., Boduch, S., 2004. Environmental Monitoring Buoy and Mooring with Telemetry. Sea Technol. 45, 14–19.

M. Bardestani, O.M. Faltinsen, A Two-Dimensional Approximation of a Floating Fish Farm in Waves and Current With the Effect of Snap Loads, (2013). https://doi.org/10.1115/OMAE2013-10487.

Hsu, W.T., Thiagarajan, K.P., Manuel, L., 2018. Snap load criteria for mooring lines of a floating offshore wind turbine. In: ASME 2018 1st Int. Offshore Wind Tech. Conf. IOWTC 2018., pp. 1–9. https://doi.org/10.1115/IOWTC2018-1047.

Palm, J., Paredes, G.M., Pinto, F.T., Bergdahl, L., 2013. Simulation of Mooring Cable Dynamics Using a Discontinuous Galerkin Method, Int. Conf. Comput. Methods Mar. Eng. - Mar 1–12.

Palm, J., Eskilsson, C., Bergdahl, L., 2017. An hp-adaptive discontinuous Galerkin method for modelling snap loads in mooring cables. Ocean Eng. 144, 266–276. https://doi.org/10.1016/j.oceaneng.2017.08.041.

Palm, J., Eskilsson, C., 2020. Influence of Bending Stiffness on Snap Loads in Marine Cables: A Study Using a High-Order Discontinuous Galerkin Method. J. Mar. Sci. Eng. 8, 795. https://doi.org/10.3390/jmse8100795.

Hsu, W., Thiagarajan, K.P., Manuel, L., 2017. Extreme mooring tensions due to snap loads on a floating offshore wind turbine system. Mar. Struct. 55, 182–199. https://doi.org/10.1016/j.marstruc.2017.05.005.

Qiao, D., Yan, J., Liang, H., Ning, D., Li, B., Ou, J., 2020. Analysis on snap load characteristics of mooring line in slack-taut process. Ocean Eng. 196, 106807 https://doi.org/10.1016/j.oceaneng.2019.106807.

Raman-Nair, W., Colbourne, B., 2003. Dynamics of a mussel longline system. Aquac. Eng. 27, 191–212. https://doi.org/10.1016/S0144-8609(02)00083-3.

Raman-Nair, W., Colbourne, B., Gagnon, M., Bergeron, P., 2008. Numerical model of a mussel longline system: Coupled dynamics. Ocean Eng. 35, 1372–1380. https://doi.org/10.1016/j.oceaneng.2008.05.008.

Kane, T.R., Levinson, D.A., 1985. Dynamics: Theory and Applications. McGraw-Hill, New York. https://doi.org/10.1016/0094-114x(86)90059-5.

Morison, J.R., O'Brien, M.P., Johnson, J.W., Schaaf, S.A., O'Brien, M.P., Johnson, J.W., Schaaf, S.A., 1950. The forces exerted by surface waves on piles. Pet. Trans. AIME. 189, 149–157.

Zhao, Y.-P., Yang, H., Bi, C., Chen, Q.-P., Dong, G.-H., Cui, Y., 2019. Hydrodynamic responses of longline aquaculture facility with lantern nets in waves. Aquac. Eng. 86, 101996 https://doi.org/10.1016/j.aquaeng.2019.101996.

Cheng, W., Sun, Z., Liang, S., Liu, B., 2020. Numerical model of an aquaculture structure under oscillatory flow. Aquac. Eng. 89, 102054 https://doi.org/10.1016/j.aquaeng.2020.102054.

Huang, C., Tang, H., Liu, J., 2006. Dynamical analysis of net cage structures for marine aquaculture : Numerical simulation and model testing. Aquac. Eng. 35, 258–270. https://doi.org/10.1016/j.aquaeng.2006.03.003.

Huang, C., Pan, J., 2010. Aquacultural Engineering Mooring line fatigue : a risk analysis for an SPM cage system. Aquac. Eng. 42, 8–16. https://doi.org/10.1016/j.aquaeng.2009.09.002.

Knysh, A., Tsukrov, I., Chambers, M., Swift, M.R., Sullivan, C., Drach, A., 2020. Numerical modeling of submerged mussel longlines with protective sleeves. Aquac. Eng. 88, 102027 https://doi.org/10.1016/j.aquaeng.2019.102027.

Bi, C.-W., Zhao, Y.-P., Dong, G.-H., Xu, T.-J., Gui, F.-K., 2014. Numerical simulation of the interaction between flow and flexible nets. J. Fluids Struct. 45, 180–201. https://doi.org/10.1016/j.jfluidstructs.2013.11.015.

Bi, C.-W., Zhao, Y.-P., Dong, G.-H., Wu, Z.-M., Zhang, Y., Xu, T.-J., 2018. Drag on and flow through the hydroid-fouled nets in currents. Ocean Eng. 161, 195–204. https://doi.org/10.1016/j.oceaneng.2018.05.005.

Bi, C.-W., Chen, Q.-P., Zhao, Y.-P., Su, H., Wang, X.-Y., 2020b. Experimental investigation on the hydrodynamic performance of plane nets fouled by hydroids in waves. Ocean Eng. 213, 107839 https://doi.org/10.1016/j.oceaneng.2020.107839.

Plew, D.R., Stevens, C.L., Spigel, R.H., Hartstein, N.D., 2005. Hydrodynamic implications of large offshore mussel farms. IEEE J. Ocean. Eng. 30, 95–108. https://doi.org/10.1109/JOE.2004.841387.

Stevens, C.L., Plew, D.R., Smith, M.J., Fredriksson, D.W., 2007. Hydrodynamic forcing of long-line mussel farms: Observations. J. Waterw. Port, Coast. Ocean Eng. 133, 192–199. https://doi.org/10.1061/(ASCE)0733-950X(2007)133:3(192).

Gagnon, M., Bergeron, P., 2017. Observations of the loading and motion of a submerged mussel longline at an open ocean site. Aquac. Eng. 78, 114–129. https://doi.org/10.1016/j.aquaeng.2017.05.004.

Heasman, K., Scott, N., Smeaton, M., Goseberg, N., Hildebrandt, A., Vitasovich, P., Elliot, A., Mandeno, M., Buck, B.H., 2020b. New system design for the cultivation of extractive species at exposed sites - Part 1: System design, deployment and first response to high-energy environments. J. Appl. Mar. Sci. (IN REVIEW).

Stolle, J., Nistor, I., Goseberg, N., Mikami, T., Shibayama, T., 2017. Entrainment and Transport Dynamics of Shipping Containers in Extreme Hydrodynamic Conditions. Coast. Eng. J. 59, 1750011–1750030. https://doi.org/10.1142/S0578563417500115.

James, S.C., O'Donncha, F., 2019. Drag coefficient parameter estimation for aquaculture systems. Environ. Fluid Mech. 19, 989–1003. https://doi.org/10.1007/s10652-019-09697-7.

J.M. Zhan, X.P. Jia, Y.S. Li, M.G. Sun, G.X. Guo, Y.Z. Hu, Analytical and experimental investigation of drag on nets of fish cages, 35 (2006) 91–101. https://doi.org/10.1016/j.aquaeng.2005.08.013.

I.M. Strand, Z. Volent, Modelling of drag forces on a closed flexible fish cage, (2013). https://doi.org/10.3182/20130918-4-JP-3022.00014.

Lawless, J.F., 2011. Statistical Models and Methods For Lifetime Data. John Wiley & Sons.

D.A. Potts, J.R. Binns, H. Marcollo, The effect of aspect ratio on the drag of bare cylinders OMAE2019-96431, (2019). https://doi.org/10.1115/OMAE2019-96431.

Lu, W., Ge, F., Wang, L., Wu, X., Hong, Y., 2011. On the slack phenomena and snap force in tethers of submerged floating tunnels under wave conditions. Mar. Struct. 24, 358–376. https://doi.org/10.1016/j.marstruc.2011.05.003.

Qin, H., Xu, Z., Li, P., Yu, S., 2020. A physical model approach to nonlinear vertical accelerations and mooring loads of an offshore aquaculture cage induced by wave-structure interactions. Ocean Eng. 197, 106904 https://doi.org/10.1016/j.oceaneng.2019.106904.

Newkirk, G.F., Muise, B.C., Enright, C.E., 1995. Culture of the Belon oyster.

Pogoda, B., Buck, B.H., Hagen, W., 2011. Growth performance and condition of oysters (Crassostrea gigas and Ostrea edulis) farmed in an offshore environment (North Sea, Germany). Aquaculture 319, 484–492. https://doi.org/10.1016/j.aquaculture.2011.07.017.

Mueller Loose, S., Peschel, A., Grebitus, C., 2013. Quantifying effects of convenience and product packaging on consumer preferences and market share of seafood products: The case of oysters. Food Qual. Prefer. 28, 492–504. https://doi.org/10.1016/j.foodqual.2012.11.004.

Matthiessen, G.C., 2001. Oyster Culture. Wiley Online Library, London.

Brenner, M., Buck, B.H., 2010. Attachment properties of blue mussel (Mytilus edulis L.) byssus threads on culture-based artificial collector substrates. Aquac. Eng. 42, 128–139. https://doi.org/10.1016/j.aquaeng.2010.02.001.

Babarro, J.M.F., Carrington, E., 2013. Attachment strength of the mussel Mytilus galloprovincialis: effect of habitat and body size. J. Exp. Mar. Bio. Ecol. 443, 188–196. https://doi.org/10.1016/j.jembe.2013.02.035.

Gordelier, T., Parish, D., Thies, P.R., Johanning, L., 2015. A novel mooring tether for highly-dynamic offshore applications; mitigating peak and fatigue loads via selectable axial stiffness. J. Mar. Sci. Eng. 3, 1287–1310. https://doi.org/10.3390/jmse3041287.

Dong, G.H.H., Zheng, Y.N.N., Li, Y.C.C., Teng, B., Guan, C.T.T., Lin, D.F.F., 2008. Experiments on wave transmission coefficients of floating breakwaters. Ocean Eng. 35, 931–938. https://doi.org/10.1016/j.oceaneng.2008.01.010.